ChemSusChem

Research Article
doi.org/10.1002/cssc.202300800

Chemistry Europe
European Chemical Societies Publishing

www.chemsuschem.org

$CuBO_2$: A Potential Alternative for NiO as a Hole Acceptor Layer

Kaijian Zhu,[a] Guido Mul,[a] and Annemarie Huijser*[a]

P-type metal oxides, and in particular NiO, are typically used as hole accepting layers in dye-sensitized photocathodes. Delafossites ($CuMO_2$) with M=B, Al, Cr or Ga have recently been proposed as attractive substitutes for NiO, with theoretically a higher hole mobility than NiO, therefore allowing a higher efficiency when the photocathode is applied in solar to fuel devices. We have experimentally validated the photoelectrochemical performance of photocathodes consisting of nanoporous $CuBO_2$ (CBO) on Fluorine-doped Tin Oxide substrates, photosensitized with a light absorbing P1 dye. Femtosecond transient absorption and time-resolved photoluminescence studies show that light-induced hole injection occurs from the P1 dye into the CBO in a few ps, comparable to the time constant observed for NiO-based photocathodes. Importantly, the CBO-based photocathode shows significantly slower charge recombination than the NiO-based analogue. These results illustrate the promise of CBO as a p-type semiconductor in solar energy conversion devices.

Introduction

The development of efficient dye-sensitized electrodes is important for the conversion of solar energy into electricity or solar fuels.[1–3] Although dye-sensitized photocathodes for solar fuel generation have been studied for more than a decade,[4] their performance is still insufficient for applications including solar water splitting and CO_2 reduction.[1,5–7] An important component of a dye-sensitized photocathode is the nanoporous wide bandgap semiconductor layer, to facilitate light-induced charge (hole) transfer from the dye into the semiconductor and further into the back-contact of the electrode, typically composed of transparent Fluorine-doped Tin Oxide. Furthermore a catalyst is typically co-adsorbed on the photoelectrode surface, connected to the photosensitizing dye, or present in the aqueous electrolyte,[8–10] which after electron transfer from the dye either reduces protons to generate H_2, or CO_2 to generate formate, CO, or hydrocarbons. Significant efforts have been made to design photosensitizers and catalysts to improve the efficiency of the photocathode.[11–14] So called "push-pull" dyes have especially been designed to improve the charge separation efficiency,[15,16] while the chemical structure of the anchoring group has been modified to promote photo-induced hole injection in the p-type semiconductor and to improve the photocathode stability.[17,18] Furthermore, dye-catalyst assemblies have been developed to improve electron transfer to the catalyst and suppress charge recombination.[19,20] Nevertheless, both time-resolved spectroscopy and computational studies provide evidence that NiO,[21–23] the widely used p-type semiconductor in dye-sensitized photocathodes, is the limiting factor to realize high efficiencies.[1] This limitation likely arises from a combination of fast surface charge recombination and a low bulk hole mobility.[24,25]

NiO shows p-type character due to the presence of Ni^{3+} defects,[26] while the intra-gap trap states resulting from Ni^{3+} or Ni^{4+} defects have been suggested to be the reason for the fast charge recombination.[27,28] The nature of the O 2p derived valence band of NiO[26] leads to hole localization and a poor hole mobility.[26] Furthermore, the NiO surface is highly sensitive to the presence of water causing surface hole accumulation. Combined with the sluggish hole conductivity in the NiO bulk, this promotes fast charge recombination.[21,29,30] In addition, the valence band position of NiO is rather high, which limits the maximum output photovoltage.[31] Therefore, it is crucial to find an alternative p-type semiconductor with high optical transparency, chemical stability, suitable valence band position and a high hole mobility.

In the quest for suitable alternative p-type semiconductor materials, delafossites ($CuMO_2$, with M=B, Al, Cr, Ga,…) have been proposed to be promising alternatives for NiO.[31–36] The hybridization of Cu 3d orbitals with O 2p orbitals likely promotes the hole delocalization and conductivity.[37–39] According to theoretical studies, a decrease in ionic radius of the M site leads to a larger bandgap and higher conductivity of $CuMO_2$,[40,41] suggesting that especially $CuBO_2$ (CBO) is promising. Research on p-type semiconductor materials has been reviewed previously.[34,42,43] Importantly, CBO shows a 10 times higher hole mobility than other $CuMO_2$ analogues and NiO, combined with a deeper valence band position.[41] Therefore, CBO is theoretically the best among the reported $CuMO_2$ candidates to replace NiO. Note that whether $CuBO_2$ is a delafossite structure is unknown, and more work should be done to have a clear view of the structure.[44] $CuBO_2$ has the

[a] Dr. K. Zhu, Prof. G. Mul, Dr. A. Huijser
PhotoCatalytic Synthesis Group, MESA + Institute for Nanotechnology
University of Twente
P.O. Box 217, 7500 AE Enschede (The Netherlands)
E-mail: j.m.huijser@utwente.nl

Supporting information for this article is available on the WWW under https://doi.org/10.1002/cssc.202300800

potential to be an excellent p-type material due to its small hole effective mass.[44] However, to the best of our knowledge, this material has hardly been studied experimentally, only one paper reports the use of CBO in a dye-sensitized photocathode of a solar cell.[45] Reproducible synthesis of CBO is challenging, and the fundamental understanding of the performance of CBO is limited. In earlier work, CBO was prepared as (dark) green colored powders, making it difficult to realize an optically transparent film suitable for dye sensitization.[45,46] Furthermore, the powders have a relatively high amount of impurities and are based on large particles, which is not suitable for application in a dye-sensitized photocathode requiring a large surface area. In addition, to the best of our knowledge there is no experimental evidence yet, neither from ultrafast spectroscopy nor photoelectrochemical studies, that CBO can indeed replace NiO.

In this work, we present a new procedure using a spin-coating technique modified relative to earlier methods,[45] enabling to make semi-transparent CBO films showing a large surface area with a nanoparticle size around 10–20 nm. We observed that the CuO impurities in the CBO films can be moderated by adjusting the precursor, the annealing temperature and annealing time. Ultrafast spectroscopy studies show that charge recombination in the CBO-based photocathode is significantly slower than in the NiO-based analogue. Photoelectrochemical experiments demonstrate the potential of CBO to replace NiO in dye-sensitized photocathodes.

Results and Discussion

Film characterization

An important challenge in the preparation of CBO is the formation of impurities.[45] Figure 1 shows the XRD patterns of various drop-coated CBO films. Figure 1a shows the CBO sample prepared from precursor solutions with different amounts of citric acid (CA) and annealed at 450 °C. Increasing the CA concentration leads to sharp XRD diffraction lines at 36.4° and 42.3°, and a line of lower intensity at 61.4°, which can be assigned to $CuBO_2$ according to JCPDS card number PDF#28-1256. With an increase in the annealing temperature to 500 °C, the sample prepared after addition of 0.004 mol CA to the precursor solution shows two additional diffraction lines around 35.5° and 38.7°, also assigned to $CuBO_2$.[45,47–49] However, as is clear from Figure 1b, these two diffraction lines do not match with JCPDS data for $CuBO_2$, instead the diffractogram of CuO is known to contain diffraction lines at 35.5° and 38.7° (JCPDS card number PDF#48-1548). With further increasing the annealing temperature to 550 °C, a temperature previously used,[45,49]

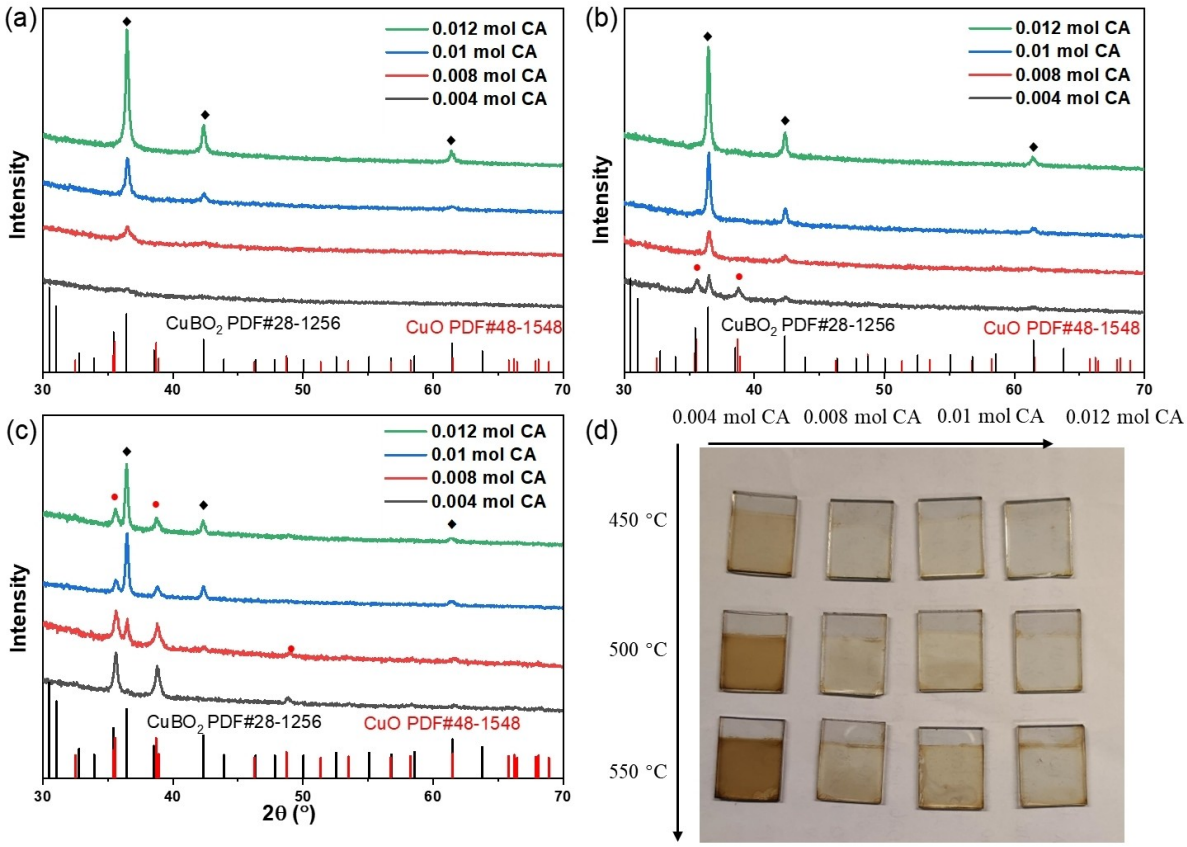

Figure 1. XRD patterns of different CBO layers prepared using four different concentrations of citric acid (CA, color legend as indicated), at 450 °C (a), 500 °C (b) and 550 °C (c); Digital photographs of CBO films with different amount of citric acid added to the precursor solution and various annealing temperatures for 1 h (d).

the diffraction lines at 36.4° and 42.3° become weaker or even disappear for the lowest CA amount added to the precursor solution, and instead diffraction lines at 35.5° and 38.7° appear. It is hence clear from Figures 1a–c that a higher annealing temperature and lower CA concentration lead to a change in diffraction lines from 36.4° and 42.3°, to 35.5° and 38.7°. Furthermore, the color of the films becomes darker along with these changes (Figure 1d). As CuO is a black narrow bandgap semiconductor material,[50] it is reasonable to assume that the higher annealing temperature and lower CA amount in the precursor solution cause phase segregation and lead to the formation of CuO impurities. We found that a further increase in the CA concentration does not result in any significant changes. Therefore, we decided to use a fixed CA amount of 0.012 mol added to the precursor solution and annealed it in the following experiments at 500 °C for 1 hour. XPS was used to investigate the oxidation states of the CBO film, the Cu 2p spectrum is shown in Figure 2. It is obvious that the surface and sub-surface (around 20 nm depth) of the film have different Cu oxidation states. On the surface, the strong satellite peaks around 942 eV and 962 eV indicate the existence of Cu^{2+}.[51] The peaks around 933.5 eV and 953.5 eV can be assigned to a mixture of Cu^{2+} and Cu^{+}.[51,52] The satellite peaks vanish by Ar^{+} sputtering, and the XPS peaks shift from 933.5 eV and 953.5 eV, to 932.7 eV and 952.7 eV. The latter indicates the presence of mainly Cu^{+} in the sub-surface,[52,53] in agreement with the oxidation state of Cu in $CuBO_2$. Note that Ar^{+} sputtering may also give reduction of Cu^{2+} in the bulk. The difference between the Cu surface and sub-surface oxidation states is likely due to surface segregation during annealing, which was reported to occur in other inorganic thin film materials.[54,55] The ratio of surface Cu:B in the presence of either 0.012 mol or 0.004 mol CA has also been analyzed by XPS and is presented in Table S1. The surface Cu:B ratio in the CBO sample prepared with 0.012 mol CA is around 1, with some spots with a higher Cu concentration possibly due to the phase segregation. In the presence of 0.004 mol CA during preparation this surface ratio is much higher, in agreement with the additional CuO phase shown by XRD (Figure 1b).

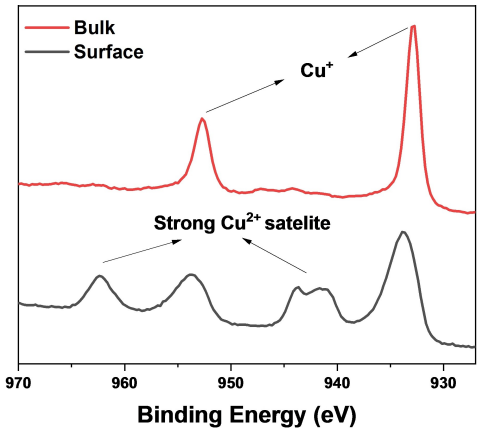

Figure 2. Cu 2p XPS spectra of the CBO film at different depth.

In addition to impurities, large particle sizes (μm size, see Figure S1) leading to a small surface area is a second important challenge to overcome for the application of $CuMO_2$ materials in dye-sensitized electrodes.[45,56] Adding F108 to the precursor solution and post-annealing to burn off the polymer results in a network structure with small nanoparticle sizes (around 10–20 nm, Figure 3a), which is ideal for dye sensitization. However, due to the strong acidity of the precursor solution, multiple spin-coating steps cannot easily increase the thickness of the film. The CBO layer obtained after one spin-coating step is very thin (around 45 nm, Figure 3b). Though this thickness is less attractive for application in a dye-sensitized photocathodes due to the limited quantity of dye which can be loaded onto the surface, the CBO layer can be used to characterize the photo-physical properties as a hole accepting material. The UV-vis spectra of the CBO films on FTO before and after photo-sensitization with a P1 dye are shown in Figure S2. It is possible to adsorb the P1 dye on the CBO surface (Figure S2), albeit with a low absorbance due to the thin film. The maximum light absorption efficiency F_A of P1 on the CBO film, corrected for the CBO background signal, is around 10% as shown in Figure S4.

The valence band (VB) position is an important factor in DSSC (dye-sensitized solar cells) and DSPEC (dye-sensitized photoelectrochemical cells), because it determines the open circuit potential V_{oc} of the device. One of the major problems for the application of NiO is its VB position, which is not deep enough to give a high V_{oc}. In contrast, CBO was reported to

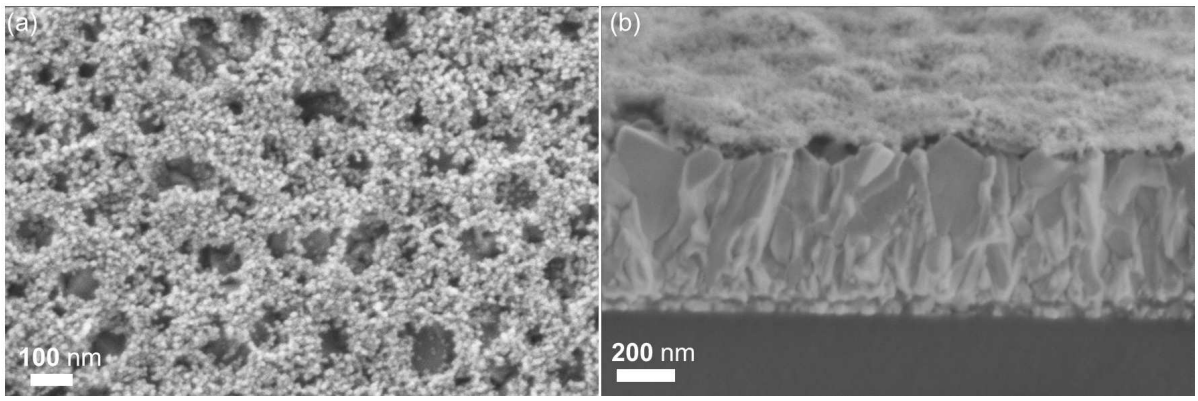

Figure 3. Surface (a) and cross-sectional (b) scanning electron micrographs of the CBO film on FTO.

have a ca. 0.75 V deeper VB than NiO.[34] Figure 4 presents Mott-Schottky plots for NiO (a) and CBO (b). The negative slopes for both NiO and CBO indicate p-type semiconductor behavior. The flat band potentials of NiO and CBO equal 0.05 V and 0.60 V vs. Ag/AgCl, respectively, suggesting a much deeper VB position for CBO. As the energy difference between the NiO VB and the P1 HOMO is around 0.9 V,[57] photoinduced hole injection in CBO/P1 should be energetically allowed.

Photodynamics

Although CBO has a deeper valence band position than NiO, a dye-sensitized solar cell based on a functionalized CBO photocathode was reported to show a more than 10 times lower short-circuit current than the NiO-based analogue.[45] Whether efficient light-induced hole injection from a dye into the CBO is possible hence remains a key question. Time-resolved photoluminescence spectroscopy is a powerful tool to probe this process, as the occurrence of light-induced charge transfer quenches the photoluminescence of the dye. Figure 5 shows the time-resolved photoluminescence spectra and decay of P1 on quartz and on CBO after 532 nm excitation. Note that CBO does not give any detectable photoluminescence under these conditions, the signals here hence mainly originate from the P1 dye. In contrast to P1 on quartz, which exhibits a long-lived PL signal with an exponential decay (Figures 5a, d), P1 on CBO shows negligible signal after the instrumental response time (Figure 5b). The decay of P1 on CBO has a Gaussian shape (Figure 5d), similar to P1 on NiO (Figure S5), indicating fast photoinduced hole injection from P1 into CBO within the instrumental response time of the streak camera setup. The PL spectra of CBO/P1 are slightly blue-shifted compared to P1 on quartz (Figure 5c). We observed that photoinduced twisting of the P1 dye leads to a red-shift in PL, and hole injection causing PL quenching occurs prior to twisting, which can explain the blue-shifted PL of CBO/P1 compared to P1 on quartz.

To gain more insight in the photodynamics of the CBO/P1 photocathode, femtosecond transient absorption (TA) studies were performed. Figure 6a and b show the TA spectra of NiO/P1 and CBO/P1 in air at various time delays after excitation at 500 nm, with the data for NiO/P1 in agreement with earlier work.[21,38,57] The TA signal below 520 nm is negligible (Figure S6) and with low signal to noise quality due to scattering by the semiconductor or low dye loading and therefore not shown here. The photoinduced ground state bleach of the P1 dye gives a broad negative signal below ca. 600 nm mirroring the absorption spectrum. The P1 excited state (P1*) is known to absorb around 560 nm (positive signal). Due to hole injection from P1* into the NiO, the intensity of the P1* signal will decrease alongside with an increase in the characteristic absorption of $P1^{\bullet-}$ around 610 nm,[57] resulting in a red-shift in the TA spectrum. Hole injection for NiO-based systems in air typically occurs biphasic, either ultrafast within the instrumental response time (< IRT, 100–150 fs) or in a time window of 1–20 ps.[57,58] Compared to NiO/P1, the spectra of CBO/P1 show a blue-shift and broader absorption at early times. As discussed in previous literature,[21,57] hole injection leads to a decrease in P1* signal and an increase in $P1^{\bullet-}$ signal, resulting in a red-shift in TA spectra. The positive signal observed around 560–580 nm for CBO/P1 indicates that there is P1* signal remaining after the IRT, indicating slower hole injection compared to NiO/P1. The gap between the TA kinetic traces at 527 nm and 560 nm (Figure 6c,d) is an indication for the ratio between the ultrafast and slow component,[21] the large gap indicates that for CBO/P1 in air hole injection is slow and mainly occurs in an early ps time window, as we have discussed in detail in earlier work.[21] Figure 6e compares the normalized kinetic traces of CBO/P1 and NiO/P1 at 610 nm, which signal is mainly due to $P1^{\bullet-}$[57] and indicative for the charge recombination dynamics. The CBO/P1 photocathode shows a slower decay, indicating slower charge recombination. A possible reason for the slower charge recombination is the higher hole conductivity that can be expected for CBO,[41] which reduces hole accumulation at the surface promoting recombination with $P1^{\bullet-}$. To quantify the difference in photodynamics between CBO/P1 and NiO/P1 and account for the spectral overlap in TA signals, target analysis has been performed using the open source program Glotaran. The TA data are well described by the photophysical model shown in Figure S7, which assumes that all photoinduced hole

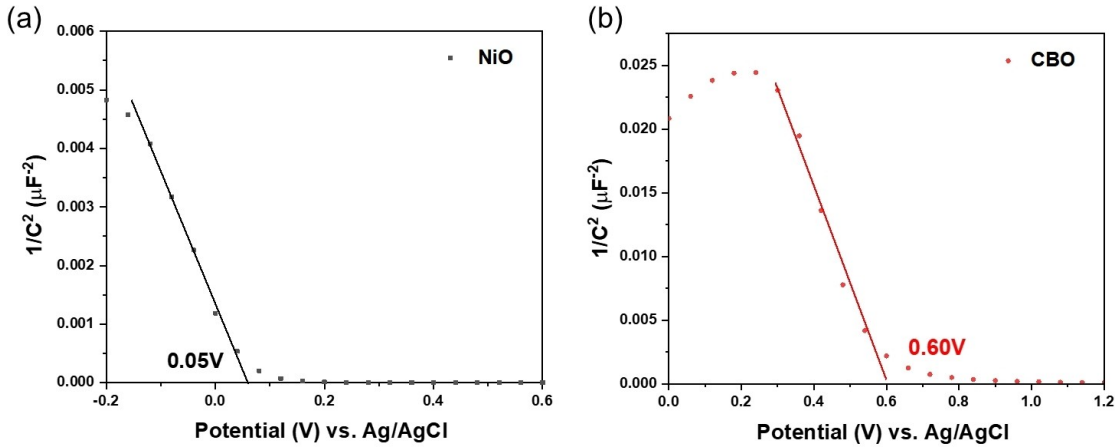

Figure 4. Mott–Schottky plots of NiO (a) and CBO (b) films measured at 1 kHz in 0.1 M PBS at pH = 7.

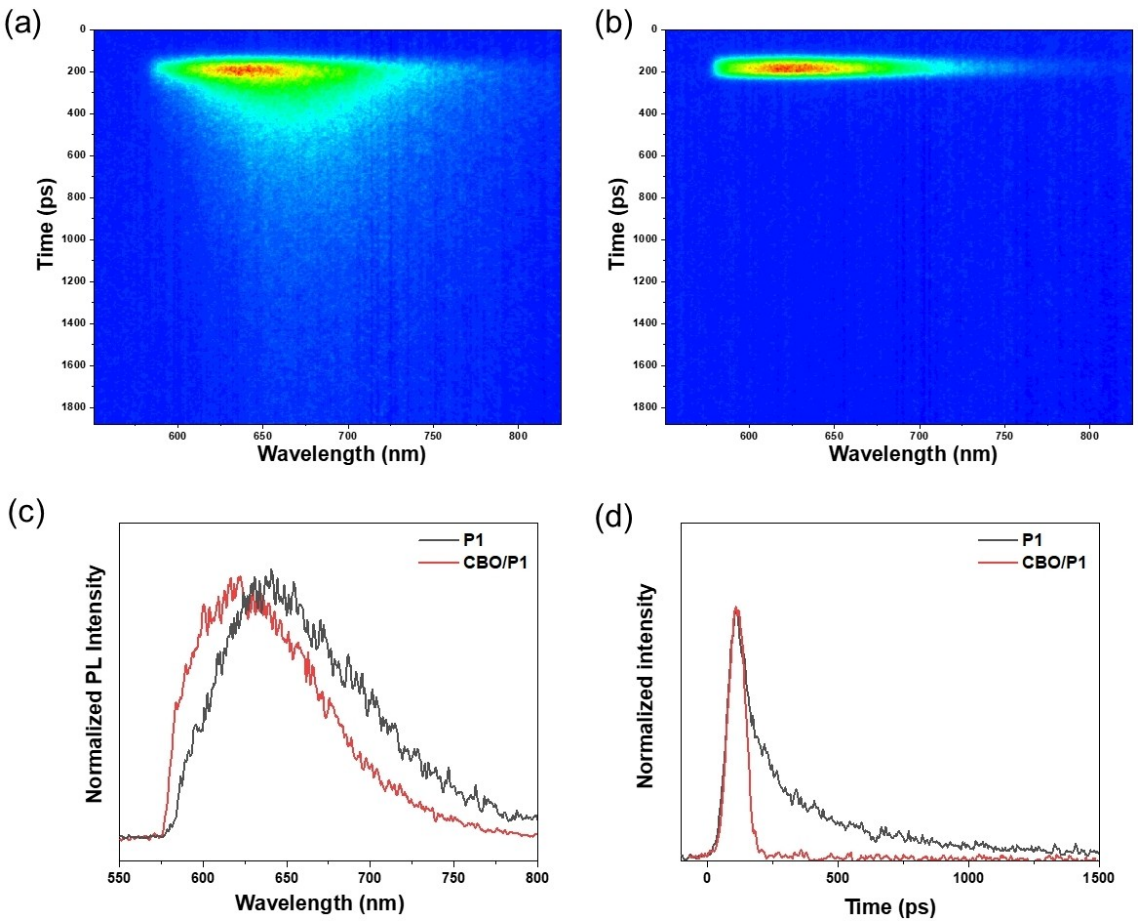

Figure 5. 2D Time-resolved photoluminescence spectral decay profiles of P1 on quartz (a) and CBO/P1 (b); Normalized photoluminescence spectra (c) and decay at 670 nm of P1 on quartz and on CBO (d), recorded using 532 nm excitation.

injection occurs in an early ps time window (τ_1 ~1 ps) and charge recombination occurs either with holes trapped at the CBO surface (τ_2) and in parallel also with relatively mobile holes which are able to reach the CBO bulk (τ_3).[38] The obtained species associated spectra and lifetimes are presented in Figure S8 and Figure 6f. Although this model is likely a simplification of the reality, it describes the TA data well, as clear from the fits included in Figure 6. Overall, these results show that from the photophysical point of view CBO is a promising potential p-type semiconductor for dye-sensitized photocathodes.

Considering that we recently observed that water has a huge impact on the NiO surface and the photoinduced charge transfer processes with P1,[21] TA studies of CBO/P1 in 0.1 M phosphate buffer solution (PBS, pH = 7) were also performed (Figure S9). The much smaller gap between the transient signals at 527 nm and 560 nm as compared to Figure 6d indicates that aqueous conditions accelerate photoinduced hole injection from the P1 dye into the CBO, the same as in NiO/P1,[21] i.e. in this case most hole injection occurs within the instrumental response time (100-150 fs), but the charge recombination is still lower than NiO/P1 in air (Figure S9b). This effect is likely due to the formation of surface OH^- on the CBO, promoting light-induced hole injection as we also observed for NiO/P1.[21]

Performance as a hole transport layer

To further evaluate the performance of the P1-sensitized CBO photocathode, the photocurrent was measured in 0.1 M phosphate buffer solution (PBS, pH = 7) with an Ag/AgCl reference electrode and an Au counter electrode. Figure 7a shows the current with chopped illumination while decreasing the applied potential from +0.1 V to −0.7 V vs. Ag/AgCl. Clearly a minimum can be observed in the j-V curve around −0.15 V, which we assign to (partial) reduction of copper oxide. The bare CBO film does not show a significant photoresponse after stabilizing, only after photosensitization with the P1 dye a photocurrent is observed. The photoresponse is best analyzed at applied potentials more negative than −0.2 V, and includes a capacitive current at −0.25 V.[59,60] Not considering this capacitive current, the photocurrent is approximately 15 μA/cm^2 at −0.25 V, while decreasing to 10 μA/cm^2 at −0.35 V. This decrease also appears in other NiO based photoelectrode[61] and is hard to explain and is likely associated with voltage dependent surface compositional changes, such as the degree of hydroxylation. The photocurrent of CBO/P1 is more clearly apparent in chronoamperometry, at 10 μA/cm^2 at −0.35 V vs. Ag/AgCl (see Figure 6b), with only maximal 10% light absorption efficiency (Figure S4).

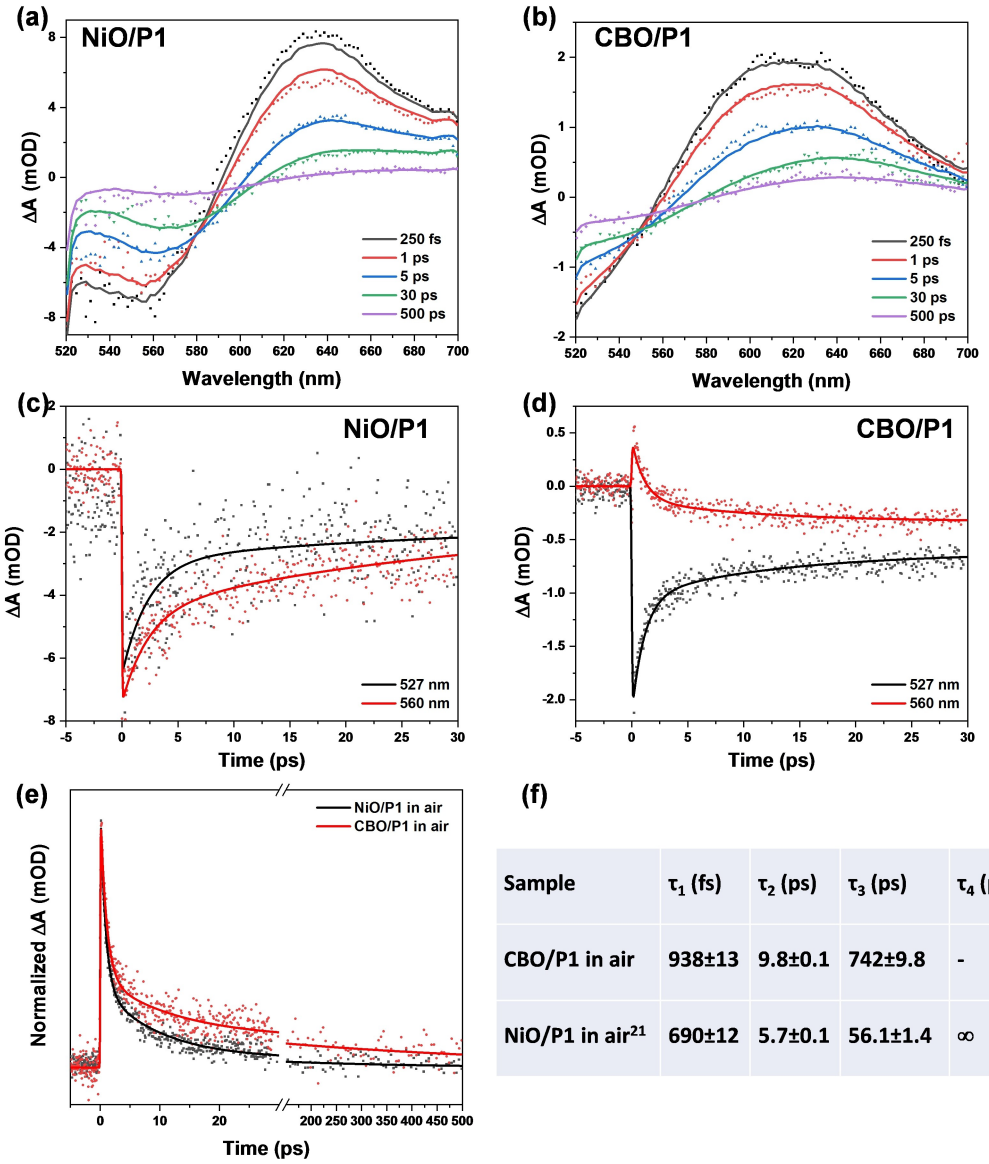

(f)

Sample	τ_1 (fs)	τ_2 (ps)	τ_3 (ps)	τ_4 (ps)
CBO/P1 in air	938±13	9.8±0.1	742±9.8	-
NiO/P1 in air[21]	690±12	5.7±0.1	56.1±1.4	∞

Figure 6. Transient absorption spectra at various time delays of NiO/P1 (a) and CBO/P1 (b) in air after excitation at 500 nm (a); kinetic traces at 527 nm and 560 nm (c, d) and comparison of kinetic traces of CBO/P1 and NiO/P1 in air at 610 nm (e). Lifetimes of CBO/P1 in air from target analysis and compared with NiO/P1 in air (f).

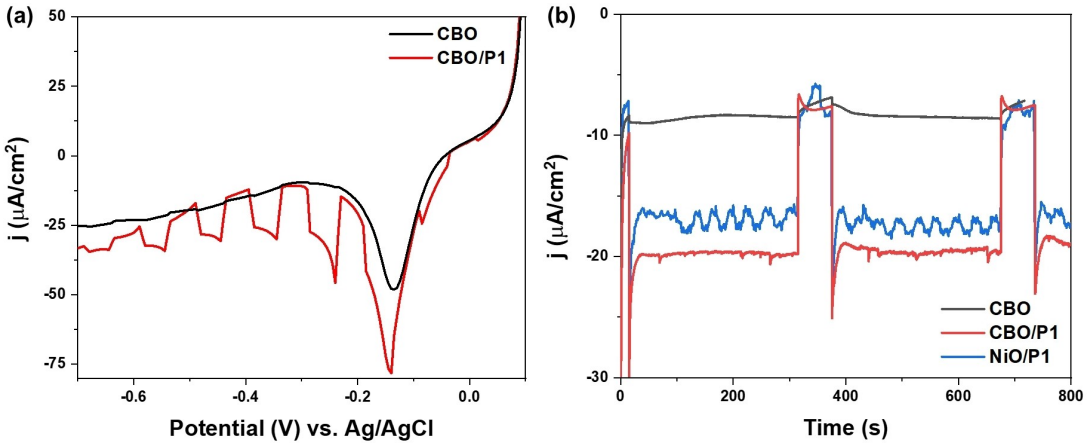

Figure 7. Photoelectrochemical performance with 1 sun backside illumination (AM 1.5G, >400 nm) of CBO and CBO/P1 in 0.1 M PBS at pH = 7. Linear sweep voltammogram with chopped illumination at 10 mV/s (a) and i-t curves at −0.35 V vs. Ag/AgCl (b).

To demonstrate the promise of the CBO-based electrode, the photocurrent of P1-sensitized NiO measured under the same conditions is included in Figure 6b. Even though the NiO is thick enough (~2 μm) enabling a high dye loading with ~90% light absorption efficiency at the P1 absorption maximum (Figure S10), the photocurrent density is similar as for CBO/P1, despite the much lower dye loading of the latter. The photocurrent density is an indication of the photocathode performance and depends on the product of light absorption, charge separation efficiency and electron injection efficiency (from the dye into the electrolyte).[62] As the electrode/electrolyte interface is the same as for NiO/P1, i.e. both P1/PBS, the photocurrent is in this case proportional to the product of the light absorption efficiency and charge separation efficiency. The approximately comparable photocurrent densities for NiO/P1 and CBO/P1, hence indicate a higher photon-to-current efficiency for the latter.

Despite the higher photon-to-current efficiency of CBO/P1 photocathodes, there are also some remaining challenges. The thickness of the CBO films limits the dye loading and therefore hinders the performance of the dye-sensitized photocathode. However, it can be potentially used as a hole transport layer instead of NiO in perovskite solar cells, in inorganic photoelectrodes or as an additional layer on top of NiO in a dye-sensitized photocathode. Figures 8a and 8b show surface and cross-sectional scanning electron micrographs of a NiO/CBO film on a FTO substrate, demonstrating that the CBO coating does not significantly change the structure of the NiO underlayer (scanning electron micrographs of NiO on FTO are shown in Figure S11), although it seems to slightly reduce the porosity. EDX mapping indicates that the CBO is uniformly coated on the NiO (Figures S11 and S12). The thickness of this NiO/CBO film allows sufficient dye loading, resulting in a light absorption efficiency higher than 90% (Figures 8c and 8d), comparable to that of NiO/P1 (Figure S10). The photocurrent density of NiO/

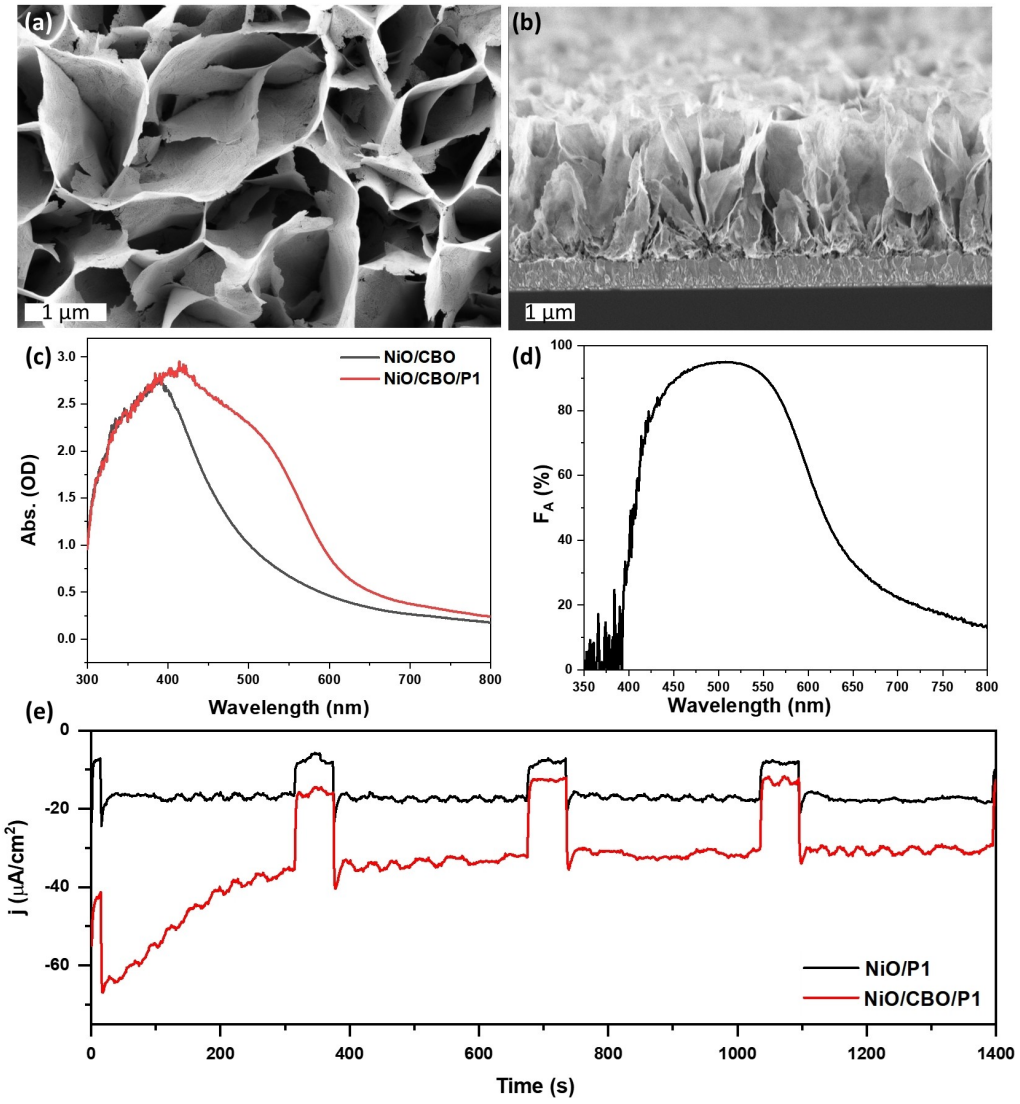

Figure 8. Surface (a) and cross-sectional (b) scanning electron micrographs of a FTO/NiO/CBO film; UV–vis absorbance spectra of a NiO/CBO layer without and with P1 dye (c); Light absorption efficiency of P1 on the NiO/CBO film corrected for the NiO/CBO background signal (d); Photoelectrochemical performance with 1 sun backside illumination (AM 1.5G, >400 nm) of NiO/CBO/P1 and NiO/P1 in 0.1 M PBS (pH = 7) at −0.35 V vs. Ag/AgCl (e).

CBO/P1 is about two-fold higher than that of NiO/P1 (Figure 8e), indicating the CBO coating reduces surface charge recombination, in agreement with Figure 6. The photocurrent drop during the initial 5 min. is likely caused by the instability of the CBO, which turns black during the measurement (Figure S13). This color change is likely due to reduction of surface CuO impurities, observed around −0.15 V vs. Ag/AgCl (Figure 7a),[63] and resulting in phase segregation. This problem could be solved by preparing a pure CBO film without any Cu^{2+} present especially at the surface (Figure 2), or attempting to move the electron away from the CBO surface prior to Cu^{2+} reduction by coating an additional electron transfer layer like TiO_2 or CdS. We should admit that this CBO material is not yet flawless, but present work demonstrates it has the potential to replace NiO as a superior hole transport layer.

Conclusions

In summary, we have prepared semi-transparent nanoporous CBO films on FTO substrates by using a sol-gel spin-coating method. The CBO film has a small particle size, suitable for application in a dye-sensitized photocathode. Photophysical analysis of a dye-sensitized CBO photocathode by time-resolved photoluminescence and femtosecond transient absorption spectroscopy demonstrate that the prepared CBO material has great potential to replace NiO, presently widely used as a p-type hole accepting metal oxide semiconductor. Photoelectrochemical studies show a comparable photocurrent as NiO/P1 analogues, even with lower dye loading on CBO, illustrating the promise of CBO in dye-sensitized photocathodes and presumably also in other solar energy conversion applications.

Experimental

Preparation of photosensitized CBO films

The CBO films were prepared by a spin-coating method. To this end, 0.004 mol $Cu(NO_3)_2 \cdot 3H_2O$ (Sigma-Aldrich, Puriss. p.a. 99–104%) was dissolved into 5 mL H_2O, and 0.002 mol B_2O_3 (Sigma-Aldrich, 99.98%) was added into a mixed solution of 5 mL H_2O and 4 mL 4 M HNO_3. Then, 0.012 mol citric acid (CA, Sigma-Aldrich, >99.5%) was added as a chelating agent to the mixed solution. Finally, 1 g of poly(ethylene glycol)-block-poly(propylene glycol)-block-poly(ethylene glycol) (F108, Sigma-Aldrich) was added to the solution to increase the viscosity for spin-coating. This precursor solution was spin-coated onto a cleaned Fluorine-doped Tin Oxide (FTO, Sigma-Aldrich) substrate using two steps: a speed of 0 rpm for 30 s. and a speed of 2000 rpm for 20 s., followed by high temperature (500 °C) annealing in air for 1 h. Drop-coating was used to prepare a film thick enough for X-ray diffraction measurements. The as-prepared CBO films were soaked in 0.3 mM 4-(bis-4-5-(2,2-dicyano-vinyl)-thiophene-2-yl-phenyl-amino)-benzoic acid (P1, Dyenamo, Sweden) dye solution in ethanol (Supelco, >99.9%) overnight (~16 h) and finally washed by ethanol (BOOM, ethanol 100%, tech.).

Preparation of NiO films

The NiO films were prepared by a chemical bath deposition method, followed by annealing. The 0.09 M $Ni(NO_3)_2 \bullet 6H_2O$ (Sigma-Aldrich, 99.999%), 0.24 M urea (Sigma-Aldrich, >99%) and 0.9 M ethanolamine (Sigma-Aldrich, >99%) precursors were sequentially dissolved into Milli-Q water. Fluorine-doped tin oxide (FTO) substrates (Sigma-Aldrich), first cleaned using acetone, isopropanol and ethanol, were put into the solution, and films were grown on the FTO at 90 °C for 3 hours and washed by milli-Q water. Finally, the NiO films were obtained by annealing in air at 450 °C for 1 hour.

Characterization

X-ray diffraction (XRD, Bruker D2, Cu Kα source) was used to determine the crystal structures. Oxidation states were characterized by X-ray Photoelectron Spectroscopy (XPS, PHI Quantes, X-ray source: Al Kα, monochromatic at 1486.6 eV). Surface sputtering was performed using a monatomic Ar^+ beam with an energy of 3 kV for 2 min. (sputtering area 2×2 mm). The binding energy of C1s = 284.6 eV was used to calibrate the spectra. The sputtering rate was estimated using a SiO_2 reference to equal 9.8 nm/min., implying that ca. 20 nm was sputtered away. The film morphology, layer thickness and energy dispersive x-ray analysis (EDX) were investigated by a high-resolution scanning electron microscope (Zeiss MERLIN HR-SEM). A ThermoSci EVO600 spectrometer was used to collect the UV-vis data, the reflectance spectrum was recorded using a PerkinElmer Lambda 950S spectrometer using an integrating sphere. The light absorption efficiency (F_A) of P1 on CBO was calculated from Equation (1):

$$F_A = (1\text{-}10^{-A}) \times 100\% \quad (1)$$

with A the absorbance in optical density (OD) of FTO/CBO/P1 corrected for the signal of FTO/CBO.

The setups used for the time-resolved photoluminescence (TRPL) and femtosecond transient absorption (TA) experiments were described in detail in previous work.[21,38] The samples were excited from the dye side. In brief, a 532 nm Fianium laser with a pulse duration of ca. 300 fs was used as the excitation source for TRPL experiments and the emission was detected using a streak camera system (Hamamatsu, C10910). The TA experiments were performed using a 500 nm pump beam, generated from the 800 nm input from a Ti:Sa amplifier (Coherent, Legend Elite, 5 kHz repetition rate, pulse duration of 35 ± 1 fs FWHM) using an optical parametric amplifier (Coherent, Opera). A small fraction of the Ti:Sa amplifier output was sent through a mechanical delay stage, focused into a CaF_2 crystal (Newlight Photonics, 3 mm thickness) mounted on a continuously moving stage to avoid crystal damage, and finally though a 700 nm short-pass filter to generate the broadband probe. The relative polarizations of the pump and probe beams were set at 54.7° magic angle. TA data analysis was performed using the program Glotaran.[64]

A VersaSTAT 3 potentiostat was used to evaluate the photoelectrochemical characteristics of a three-electrode cell under backside irradiation (i.e. through the glass/TCO) using a solar simulator equipped with an AM 1.5G filter (Newport, 1 sun intensity) and a filter blocking the UV component (<400 nm). An Au wire was used as the counter electrode, while an Ag/AgCl electrode was used as the reference electrode. Prior to the measurements, the phosphate buffer solution (PBS, pH = 7) was degassed by N_2 for more than 20 min. The data were performed using a scan rate of 5 mV/s, and scans were recorded from high to low potential. The Mott–Schottky plots were measured at room

temperature with the same cell and electrolyte using a BioLogic VSP potentiostat.

Supporting Information

The authors have cited additional references within the Supporting Information.[65–66]

Acknowledgements

The authors would like to acknowledge Jeroen P. Korterik (University of Twente) for technical support, and Prof. Bastian Mei (presently at Ruhr University Bochum, until recently at University of Twente) for scientific discussions. This work is a part of the Advanced Research Center for Chemical Building Blocks, ARC CBBC, which is co-founded and co-financed by the Netherlands Organization for Scientific Research (NWO) and the Netherlands Ministry of Economic Affairs and Climate Policy.

Conflict of Interests

The authors declare no conflict of interest.

Data Availability Statement

The data that support the findings of this study are available from the corresponding author upon reasonable request.

Keywords: Photocathode · hole transport layer · photodynamics · p-type semiconductor · $CuBO_2$

[1] A. B. Muñoz-García, I. Benesperi, G. Boschloo, J. J. Concepcion, J. H. Delcamp, E. A. Gibson, G. J. Meyer, M. Pavone, H. Pettersson, A. Hagfeldt, M. Freitag, *Chem. Soc. Rev.* **2021**, *50*, 12450–12550.
[2] S. Yun, N. Vlachopoulos, A. Qurashi, S. Ahmad, A. Hagfeldt, *Chem. Soc. Rev.* **2019**, *48*, 3705–3722.
[3] H. L. Wu, X. B. Li, C. H. Tung, L. Z. Wu, *Adv. Sci.* **2018**, *5*, 1700684.
[4] L. Li, L. L. Duan, F. Y. Wen, C. Li, M. Wang, A. Hagfeld, L. C. Sun, *Chem. Commun.* **2012**, *48*, 988–990.
[5] B. Shan, M. K. Brennaman, L. Troian-Gautier, Y. Liu, A. Nayak, C. M. Klug, T.-T. Li, R. M. Bullock, T. J. Meyer, *J. Am. Chem. Soc.* **2019**, *141*, 10390–10398.
[6] K. A. Click, D. R. Beauchamp, Z. Huang, W. Chen, Y. Wu, *J. Am. Chem. Soc.* **2016**, *138*, 1174–1179.
[7] Y. Zhu, D. Wang, Q. Huang, J. Du, L. Sun, F. Li, T. J. Meyer, *Nat. Commun.* **2020**, *11*, 4610.
[8] V. Nikolaou, A. Charisiadis, G. Charalambidis, A. G. Coutsolelos, F. Odobel, *J. Mater. Chem. A* **2017**, *5*, 21077–21113.
[9] C. E. Castillo, M. Gennari, T. Stoll, J. Fortage, A. Deronzier, M.-N. Collomb, M. Sandroni, F. Légalité, E. Blart, Y. Pellegrin, *J. Phys. Chem. C* **2015**, *119*, 5806–5818.
[10] A. Moinel, M. Brochnow, C. Aumaître, E. Giannoudis, J. Fize, C. Saint-Pierre, J. Pécaut, P. Maldivi, V. Artero, R. Demadrille, *Sustain. Energy Fuels* **2022**, *6*, 3565–3572.
[11] E. A. Gibson, *Chem. Soc. Rev.* **2017**, *46*, 6194–6209.
[12] J. Sun, Y. Wu, *Angew. Chem. Int. Ed.* **2020**, *132*, 10996–11000.
[13] J. Huang, J. Sun, Y. Wu, C. Turro, *J. Am. Chem. Soc.* **2021**, *143*, 1610–1617.
[14] L. Wang, D. E. Polyansky, J. J. Concepcion, *J. Am. Chem. Soc.* **2019**, *141*, 8020–8024.
[15] A. Nattestad, A. J. Mozer, M. K. Fischer, Y.-B. Cheng, A. Mishra, P. Bäuerle, U. Bach, *Nat. Mater.* **2010**, *9*, 31–35.
[16] E. A. Gibson, A. L. Smeigh, L. Le Pleux, J. Fortage, G. Boschloo, E. Blart, Y. Pellegrin, F. Odobel, A. Hagfeldt, L. Hammarström, *Angew. Chem. Int. Ed.* **2009**, *121*, 4466–4469.
[17] T.-T. Li, B. Shan, T. J. Meyer, *ACS Energy Lett.* **2019**, *4*, 629–636.
[18] K. Yun, S. Zhang, F. Yu, H. Ye, J. Hua, *J. Energy Chem.* **2018**, *27*, 728–735.
[19] E. Giannoudis, S. Bold, C. Müller, A. Schwab, J. Bruhnke, N. Queyriaux, C. Gablin, D. Léonard, C. Saint-Pierre, D. Gasparutto, *ACS Appl. Mater. Interfaces.* **2021**, *13*, 49802–49815.
[20] D. Sun, A. Morozan, M. Koepf, V. Artero, *Chem. Sci.* **2022**, *13*, 3857–3863.
[21] K. Zhu, S. K. Frehan, G. Mul, A. Huijser, *J. Am. Chem. Soc.* **2022**, *144*, 11010–11018.
[22] S. Piccinin, D. Rocca, M. Pastore, *J. Phys. Chem. C* **2017**, *121*, 22286–22294.
[23] J. Massin, M. Bräutigam, S. Bold, M. Wächtler, M. Pavone, A. B. Muñoz-García, B. Dietzek, V. Artero, M. Chavarot-Kerlidou, *J. Phys. Chem. C* **2019**, *123*, 17176–17184.
[24] N. T. Potts, T. Sloboda, M. Wächtler, R. A. Wahyuono, V. D'Annibale, B. Dietzek, U. B. Cappel, E. A. Gibson, *J. Chem. Phys.* **2020**, *153*, 184704.
[25] F. A. Black, C. A. Clark, G. H. Summers, I. P. Clark, M. Towrie, T. Penfold, M. W. George, E. A. Gibson, *Phys. Chem. Chem. Phys.* **2017**, *19*, 7877–7885.
[26] J. Zhang, W. Li, R. Hoye, J. MacManus-Driscoll, M. Budde, O. Bierwagen, L. Wang, Y. Du, M. Wahila, L. Piper, *J. Mater. Chem. C* **2018**, *6*, 2275–2282.
[27] L. D'Amario, L. J. Antila, B. Pettersson Rimgard, G. Boschloo, L. Hammarstrom, *J. Phys. Chem. Lett.* **2015**, *6*, 779–783.
[28] L. D'Amario, J. Föhlinger, G. Boschloo, L. Hammarström, *Chem. Sci.* **2018**, *9*, 223–230.
[29] A. Corani, M.-H. Li, P.-S. Shen, P. Chen, T.-F. Guo, A. El Nahhas, K. Zheng, A. Yartsev, V. Sundstrom, C. S. Ponseca Jr, *J. Phys. Chem. Lett.* **2016**, *7*, 1096–1101.
[30] A. D. Taggart, J. M. Evans, L. Li, K. J. Lee, J. L. Dempsey, Y. Kanai, J. F. Cahoon, *ACS Appl. Energ. Mater.* **2020**, *3*, 10702–10713.
[31] A. Renaud, B. Chavillon, L. Le Pleux, Y. Pellegrin, E. Blart, M. Boujtita, T. Pauporte, L. Cario, S. Jobic, F. Odobel, *J. Mater. Chem.* **2012**, *22*, 14353–14356.
[32] C. D. Windle, H. Kumagai, M. Higash, R. Brisse, S. Bold, B. Jousselme, M. Chavarot-Kerlidou, K. Maeda, R. Abe, O. Ishitani, V. Artero, *J. Am. Chem. Soc.* **2019**, *141*, 9593–9602.
[33] C. E. Creissen, J. Warnan, D. Antón-García, Y. Farré, F. Odobel, E. Reisner, *ACS Catal.* **2019**, *9*, 9530–9538.
[34] S. Wrede, H. Tian, *Phys. Chem. Chem. Phys.* **2020**, *22*, 13850–13861.
[35] M. Sun, J. Sun, C. Zhao, J. Wu, H. Gao, Y. Guo, X. Yin, Y. Lin, Z. Tian, M. He, L. Wang, *ACS Appl. Mater. Interfaces* **2022**, *14*, 13352–13360.
[36] S. Akin, F. Sadegh, S. Turan, S. Sonmezoglu, *ACS Appl. Mater. Interfaces* **2019**, *11*, 45142–45149.
[37] W. Chen, Y. Wu, J. Fan, A. B. Djurišić, F. Liu, H. W. Tam, A. Ng, C. Surya, W. K. Chan, D. Wang, *Adv. Energy Mater.* **2018**, *8*, 1703519.
[38] K. Zhu, S. K. Frehan, A. M. Jaros, D. B. O'Neill, J. P. Korterik, K. Wenderich, G. Mul, A. Huijser, *J. Phys. Chem. C* **2021**, *125*, 16049–16058.
[39] Y. Li, F. Yang, Y. Yu, *Chin. J. Catal.* **2017**, *38*, 767–773.
[40] R. Nagarajan, A. Draeseke, A. Sleight, J. Tate, *J. Appl. Phys.* **2001**, *89*, 8022–8025.
[41] M. Snure, A. Tiwari, *Appl. Phys. Lett.* **2007**, *91*, 092123.
[42] M.-H. Li, J.-H. Yum, S.-J. Moon, P. Chen, *Energies* **2016**, *9*, 331.
[43] Z. Wang, P. K. Nayak, J. A. Caraveo-Frescas, H. N. Alshareef, *Adv. Mater.* **2016**, *28*, 3831–3892.
[44] T. Cerqueira, R. Sarmiento-Pérez, F. Trani, M. Amsler, S. Goedecker, M. Marques, S. Botti, *MRS Commun.* **2013**, *3*, 157–160.
[45] T. Jiang, M. Bujoli-Doeuff, Y. Farré, E. Blart, Y. Pellegrin, E. Gautron, M. Boujtita, L. Cario, F. Odobel, S. Jobic, *RSC Adv.* **2016**, *6*, 1549–1553.
[46] S. Santra, N. Das, K. Chattopadhyay, *Mater. Res. Bull.* **2013**, *48*, 2669–2677.
[47] S. Santra, N. Das, K. Chattopadhyay, *Mater. Lett.* **2013**, *92*, 198–201.
[48] S. Santra, D. Das, N. S. Das, K. K. Nanda, *ACS Appl. Energ. Mater.* **2018**, *2*, 260–268.
[49] S. Santra, N. Das, K. Chattopadhyay, *AIP Conf. Proc.* **2013**, *1536*, 723.
[50] K. Mageshwari, R. Sathyamoorthy, *J. Mater. Sci. Technol.* **2013**, *29*, 909–914.
[51] S. Poulston, P. Parlett, P. Stone, M. Bowker, *Surf. Interface Anal.* **1996**, *24*, 811–820.

[52] M. Zhang, J. Wang, H. Xue, J. Zhang, S. Peng, X. Han, Y. Deng, W. Hu, *Angew. Chem. Int. Ed.* **2020**, *132*, 18621–18625.
[53] J. Shi, H. Liang, X. Xia, Q. Abbas, *Appl. Surf. Sci.* **2021**, *569*, 151010.
[54] W. Luo, Z. Li, T. Yu, Z. Zou, *J. Phys. Chem. C* **2012**, *116*, 5076–5081.
[55] T. Wang, W. Luo, X. Wen, Z. Zou, W. Huang, *ChemNanoMat* **2016**, *2*, 652–655.
[56] H. Kumagai, G. Sahara, K. Maeda, M. Higashi, R. Abe, O. Ishitani, *Chem. Sci.* **2017**, *8*, 4242–4249.
[57] L. Zhang, G. Boschloo, L. Hammarström, H. Tian, *Phys. Chem. Chem. Phys.* **2016**, *18*, 5080–5085.
[58] V. Maffeis, B. Jousselme, T. Gustavsson, *Photochem. Photobiol. Sci.* **2021**, *20*, 1257–1271.
[59] F. Le Formal, K. Sivula, M. Grätzel, *J. Phys. Chem. C* **2012**, *116*, 26707–26720.
[60] K. Zhu, G. Zhu, J. Wang, J. Zhu, G. Sun, Y. Zhang, P. Li, Y. Zhu, W. Luo, Z. Zou, *J. Mater. Chem. A* **2018**, *6*, 21360–21367.
[61] N. Lalaoui, M. Abdellah, K. L. Materna, B. Xu, H. Tian, A. Thapper, J. Sa, L. Hammarström, S. Ott, *Dalton Trans.* **2022**, *51*, 15716–15724.
[62] H. Dotan, K. Sivula, M. Grätzel, A. Rothschild, S. C. Warren, *Energy Environ. Sci.* **2011**, *4*, 958–964.
[63] H. Naatz, S. Lin, R. Li, W. Jiang, Z. Ji, C. H. Chang, J. Köser, J. Thöming, T. Xia, A. E. Nel, L. Mädler, S. Pokhrel, *ACS Nano* **2017**, *11*, 501–515.
[64] J. Snellenburg, S. Laptenok, R. Seger, K. M. Mullen, I. Van Stokkum, *J. Stat. Softw.* **2012**, *49*, 1–22.
[65] S. Traiphop, P. Thongbai, T. Kamwanna, *J. Aust. Ceram. Soc.* **2020**, *56*, 499–505.
[66] H. Xing, L. E. Z. Guo, D. Zhao, Z. Liu, *Chem. Eng. J.* **2020**, *394*, 124907.

Manuscript received: June 19, 2023
Revised manuscript received: September 14, 2023
Accepted manuscript online: September 14, 2023
Version of record online: November 3, 2023